

Do satellite galaxies trace matter in galaxy clusters ?

Chunxiang Wang^{1,2}, Ran Li^{1,3*}, Liang Gao^{1,3,4}, Huanyuan Shan^{5,6}, Jean-Paul Kneib^{5,7}, Wenting Wang⁸, Gang Chen², Martin Makler⁹, Maria E. S. Pereira⁹, Lin Wang^{1,3}, Marcio A.G. Maia¹⁰, Thomas Erben⁶

¹Key Laboratory for Computational Astrophysics, National Astronomical Observatories, Chinese Academy of Sciences, Beijing 100012, China

²Tianjin Astrophysics Center, Tianjin Normal University, Tianjin 300387, China

³School of Astronomy and Space Sciences, University of Chinese Academy of Sciences, 19A Yuquan Road, Beijing 100049, China

⁴Institute of Computational Cosmology, Department of Physics, University of Durham, Science Laboratories, South Road, Durham DH1 3LE, UK

⁵Laboratoire d'astrophysique (LASTRO), Ecole Polytechnique Fédérale de Lausanne (EPFL), Observatoire de Sauverny, CH-1290 Versoix, Switzerland

⁶Argelander Institute for Astronomy, University of Bonn, Auf dem Hügel 71, D-53121 Bonn, Germany

⁷Aix Marseille Université, CNRS, LAM (Laboratoire d'Astrophysique de Marseille) UMR 7326, 13388, Marseille, France

⁸Kavli IPMU (WPI), UTIAS, The University of Tokyo, Kashiwa, Chiba 277-8583, Japan

⁹Centro Brasileiro de Pesquisas Físicas - Rua Dr. Xavier Sigaud 150, CEP 22290-180, Rio de Janeiro, RJ, Brazil

¹⁰Laboratório Interinstitucional de e-Astronomia - LIneA, Rua General José Cristiano, 77, Rio de Janeiro, RJ, 20921-400, Brazil

9 January 2018

ABSTRACT

The spatial distribution of satellite galaxies encodes rich information of the structure and assembly history of galaxy clusters. In this paper, we select a redMaPPer cluster sample in SDSS Stripe 82 region with $0.1 \leq z \leq 0.33$, $20 < \lambda < 100$ and $P_{\text{cen}} > 0.7$. Using the high-quality weak lensing data from CS82 Survey, we constrain the mass profile of this sample. Then we compare directly the mass density profile with the satellite number density profile. We find that the total mass and number density profiles have the same shape, both well fitted by an NFW profile. The scale radii agree with each other within 1σ error ($r_{\text{s,gal}} = 0.34^{+0.04}_{-0.03}$ Mpc vs $r_{\text{s}} = 0.37^{+0.15}_{-0.10}$ Mpc).

Key words: cosmology: dark matter – galaxies: statistics – clusters: general – gravitational lensing: weak

1 INTRODUCTION

The spatial distribution of satellite galaxies encodes rich information of the structure of galaxy clusters/groups. In particular, the radial number density profiles of galaxy clusters have been often used to constrain galaxy formation models (e.g. Gao et al. 2004; Diemand et al. 2004; Wang et al. 2014). High-resolution simulations show that the distribution of subhalos is less concentrated than the distribution of dark matter (Gao et al. 2004; Springel et al. 2001; Vogelsberger et al. 2014). In addition, subhalos appear to have a significantly shallower radial distribution than the observed distribution of galaxies in the inner region of clusters (Gao et al. 2004). In hydrodynamical simulations, the galaxies can survive longer than the dark matter subhaloes. The dissipative processes of galaxy formation make the stellar compo-

nent more resistant to tidal disruption close to cluster centres (Vogelsberger et al. 2014). Observationally, there are lots of controversies in the literature on whether satellite galaxies unbiasedly trace the underlying mass distribution in galaxy clusters/groups. Some studies conclude that the satellite (luminosity) distribution traces the mass distribution (Tyson & Fischer 1995; Squires et al. 1996; Fischer & Tyson 1997; Cirimele et al. 1997; Carlberg et al. 1997; van der Marel et al. 2000; Rines et al. 2001; Tustin et al. 2001; Biviano & Girardi 2003; Lokas & Mamon 2003; Kneib et al. 2003; Biviano & Girardi 2003; Parker et al. 2005; Popesso et al. 2007; Sheldon et al. 2009; Wojtak & Lokas 2010; Sereno et al. 2010; Bahcall & Kulier 2014); while some studies suggest that the spatial distribution of satellites (luminosity) are less concentrated than that of matter (Rines et al. 2000; Lin et al. 2004; Hansen et al. 2005; Nagai & Kravtsov 2005; Yang et al. 2005; Budzynski et al. 2012); still some claim luminosity distribution are actually more concentrated (Koranyi et al. 1998; Carlberg et al. 2001).

* E-mail: liran827@gmail.com

Many of previous comparisons depend on probes of mass profiles based on real observational data, e.g. dynamical modeling methods (Carlberg et al. 1997; van der Marel et al. 2000; Rines et al. 2000; Carlberg et al. 2001; Rines et al. 2001; Tustin et al. 2001; Biviano & Girardi 2003; Lokas & Mamon 2003; Popesso et al. 2007), or X-ray observation (Cirimele et al. 1997; Lin et al. 2004; Budzynski et al. 2012). Mass estimation from these probes often requires some prior assumptions on the dynamical state of galaxy clusters/groups and thus may be biased. Weak lensing method is usually considered as an unbiased probe, which is independent of the dynamical states of galaxy clusters and baryonic physics in galaxy formation. In this work, we derive mass distribution of redMaPPer clusters (Rykoff et al. 2014; Rozo & Rykoff 2014) using the high-quality weak lensing data from Canada-France-Hawaii Telescope (CFHT) Stripe 82 Survey (CS82; Shan et al. 2014; Li et al. 2014), and compare them directly with the satellite galaxies number density from SDSS Stripe 82 (Abazajian et al. 2009; Reis et al. 2012) photometric data.

The paper is laid out as follows. In §2 we describe the data used in our work. In §3 we describe lens model and how to get the satellite galaxy number density profile of our cluster sample. In §4, we show the results of this work. Finally, we summarize and discuss the implication of our results in §5. Throughout this paper, we adopt a flat Λ CDM cosmological model with the matter density parameter $\Omega_m = 0.27$ and the Hubble parameter $H_0 = 70 \text{ km s}^{-1} \text{ Mpc}^{-1}$.

2 DATA

2.1 RedMaPPer cluster catalog

The red-sequence Matched-filter Probabilistic Percolation method (redMaPPer; Rozo & Rykoff 2014; Rykoff et al. 2014) uses the *ugriz* magnitudes and their errors, to group spatial concentrations of red-sequence galaxies at similar redshift into cluster. In this paper, we use redMaPPer cluster catalog extracted from SDSS DR8, restricting to the CS82 footprint, where high quality weak lensing data is available. There are 634 clusters falling in this region. We further select our final cluster sample from these clusters using the following additional conditions: $0.1 \leq z \leq 0.33$, $20 < \lambda < 100$ and $P_{\text{cen}} > 0.7$, where z is the redshift of cluster, the λ is an optical richness estimate indicating the number of red sequence galaxies brighter than $0.2L_*$ at the redshift of the cluster within a scaled aperture which has been shown as a good mass proxy (Rykoff et al. 2012), and the P_{cen} is the probability of the most likely central galaxy. For each cluster, there are five candidate central galaxies and we always use the position of the most likely central galaxy as the proxy of the cluster centre. The redshift cut selects a nearly volume-limited cluster sample, the richness cut ensures a pure and statistically meaningful sample of clusters at all richness bins (Miyatake et al. 2016) and the probability cut reduces the miscentering problem. After applying these cuts our final sample is composed of 167 clusters.

2.2 Lensing shear catalog

The source galaxies used in this work are taken from CS82 survey which is an *i*-band imaging survey covering the SDSS Stripe 82 region with a median seeing $0.59''$. The CS82 fields were observed in four dithered observation with 410 seconds exposure. The limited magnitude is $i_{\text{AB}} \sim 24.1$ (Battaglia et al. 2016).

The shapes of faint galaxies are measured with *lensfit* method (Miller et al. 2007, 2013). Each CS82 science image is supplemented by a mask, indicating regions within which accurate photometry/shape measurements of faint sources cannot be performed. According to Erben et al. (2013), most of science analysis are safe with $MASK \leq 1$. We use all galaxies with weight $\omega > 0$, FITCLASS=0, $MASK \leq 1$ and $z > 0$, in which ω represents an inverse variance weight assigned to each source galaxy by *lensfit*, FITCLASS is a star/galaxy classification provided by *lensfit*, and z is the photometric redshift.

After masking out bright stars and other image artifacts, the effective survey area reduces from 173 deg^2 to 129.2 deg^2 . As the CS82 is *i*-band imaging survey, the photometric redshifts (photo- z) are obtained by using BPZ method (Benítez 2000; Coe et al. 2006) and computed by (Bundy et al. 2015). Some tests on the systematics induced by photo- z error are shown in (Li et al. 2016). The total number of source galaxies in this work is 4,381,917.

2.3 Satellite galaxy catalog

To calculate the satellite galaxy number density of our cluster sample as described in §2.1, we download a photometric galaxy catalog from SDSS Stripe 82 database by requiring the magnitude of *r*-band (r_{mag}) in $[17, 21]$ with the query provided by Reis et al. (2012). There are 1,164,364 galaxies in the catalog. By matching this photometric catalog to the redMaPPer cluster catalog with a matching tolerance of $1.0''$, “central galaxies” are identified in this photometric catalog.

3 THEORY MODEL AND METHOD

3.1 Lensing model

We stack lens-source pairs in 7 logarithmic radial R bins from 0.03 Mpc to 1.5 Mpc. Lensing signal (excess surface density $\Delta\Sigma(R)$) is calculated by

$$\Delta\Sigma(R) = \overline{\Sigma(<R)} - \overline{\Sigma(R)} = \frac{\sum_{\text{ls}} \omega_{\text{ls}} \gamma_{\text{t}}^{\text{ls}} \Sigma_{\text{crit}}}{\sum_{\text{ls}} \omega_{\text{ls}}}, \quad (1)$$

where

$$\omega_{\text{ls}} = \omega_s \Sigma_{\text{crit}}^{-2}, \quad (2)$$

$$\Sigma_{\text{crit}} = \frac{c^2}{4\pi G} \frac{D_s}{D_1 D_{\text{ls}}}, \quad (3)$$

$\overline{\Sigma(<R)}$ is the mean surface mass density within R , $\overline{\Sigma(R)}$ is the average surface density at the projected radius R , ω_s is a weight factor introduced to account for intrinsic scatter in ellipticity and shape measurement error of each source

galaxy, which is same with ω we mentioned in §2.1, Σ_{crit} is the critical surface density including space geometry information, D_s and D_l are the angular diameter distances of source and lens, respectively, D_{ls} is the angular diameter distance between source and lens, and γ_t is the tangential shear.

We apply a correction to lensing signal computed from the multiplicative shear calibration factor m as in Velander et al. (2014):

$$1 + K(z_l) = \frac{\sum_{ls} \omega_{ls}(1+m)}{\sum_{ls} \omega_{ls}}. \quad (4)$$

Weak lensing signal can finally be obtained by:

$$\Delta\Sigma^{\text{cal}}(R) = \frac{\Delta\Sigma(R)}{1 + K(z_l)}. \quad (5)$$

Owing to large photo- z uncertainties of the source galaxies, we remove the lens-source pairs with $z_s - z_l < \sigma_z$, where σ_z represents 1σ error of photo- z .

The weak lensing signal is modeled as:

$$\Delta\Sigma(R) = \frac{M_{\text{star}}}{\pi R^2} + P_{\text{cc}}\Delta\Sigma_{\text{NFW}}(R) + (1 - P_{\text{cc}})\Delta\Sigma_{\text{NFW}}^{\text{off}}(R), \quad (6)$$

where the first term represents the contribution of the stellar mass of the central galaxy, the second and the third terms represent the perfectly centered and miscentered component of dark matter halos (and also the diffused baryonic matter like hot gas), respectively.

We model the central galaxy as a point mass following Leauthaud et al. (2012) and fix M_{star} to the average mass of central galaxies. Stellar masses are estimated for member galaxies in the redMaPPer catalog using the Bayesian spectral energy distribution (SED) modeling code ISEDFIT (Moustakas et al. 2013). P_{cc} and $(1 - P_{\text{cc}})$ are weights for the centered and miscentering part of the dark matter halo surface mass density, respectively.

Dark matter density profile is described by the Navarro et al. (1997, hereafter NFW) profile:

$$\rho(r) \propto \frac{1}{(r/r_s)(1+r/r_s)^2}, \quad (7)$$

where r_s is the scale radius which is commonly quantified in terms of the concentration parameter $C_{200} = R_{200}/r_s$, where R_{200} is the virial radius enclosing the virial mass $M_{200} = (800/3)\pi R_{200}^3 \rho_c$, where ρ_c is the critical density of the universe at the redshift of the halo.

By integrating the three-dimensional density profile along the line of sight, we can get the projected surface density $\Sigma_{\text{NFW}}(R)$ which is a function of the projection radius R :

$$\Sigma_{\text{NFW}}(R) = \int_0^\infty \rho(\sqrt{R^2 + z^2}) dz. \quad (8)$$

Integrating $\Sigma_{\text{NFW}}(R)$ from 0 to R , we can get the the mean surface density within R , $\overline{\Sigma_{\text{NFW}}(< R)}$:

$$\overline{\Sigma_{\text{NFW}}(< R)} = \frac{2}{R^2} \int_0^R R' \Sigma_{\text{NFW}}(R') dR', \quad (9)$$

here ρ is the NFW density profile.

There are possibilities that BCG may be misidentified in the cluster catalog, we also including a “*miscentering*” term. If the central galaxy is offset from the halo center by

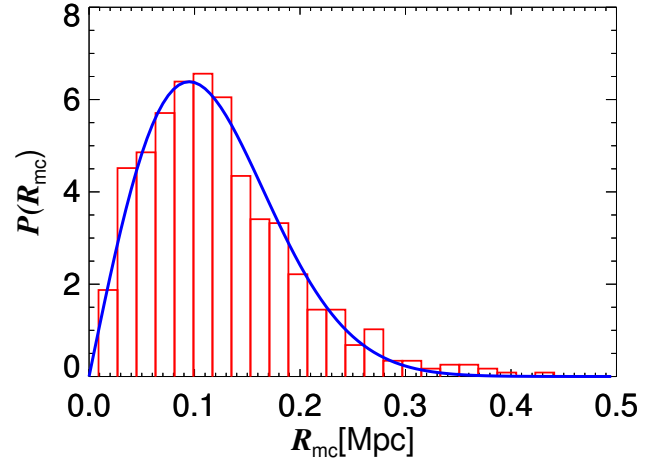


Figure 1. The distribution of miscentering. We take the projected distance between the most likely central galaxy and the 4 remaining central candidate galaxies as R_{mc} . The red histogram shows the distribution of R_{mc} . The blue line is the best fit curve of the distribution of R_{mc} .

a distance R_{mc} , the mass surface density will be changed as follow:

$$\Sigma_{\text{NFW}}(R|R_{\text{mc}}) = \int_0^{2\pi} d\theta \Sigma_{\text{NFW}} \left(\sqrt{R^2 + R_{\text{mc}}^2 + 2RR_{\text{mc}}\cos(\theta)} \right). \quad (10)$$

The distribution of miscentering can be described by a 2D Gaussian distribution:

$$P(R_{\text{mc}}) = \frac{R_{\text{mc}}}{\sigma_{\text{off}}^2} \exp\left(-\frac{1}{2}\left(\frac{R_{\text{mc}}}{\sigma_{\text{off}}}\right)^2\right). \quad (11)$$

In the fitting model there are four free parameters, M_{200} , C_{200} , σ_{off} and P_{cc} . Due to the strong degeneracy between σ_{off} and P_{cc} , our data are not good enough to fit σ_{off} and P_{cc} well synchronously (see the results in the APPENDIX A). We assume that the position of one of the five central galaxy candidates is true center of the galaxy cluster, so we fix σ_{off} and P_{cc} in following way.

First, we fix $P_{\text{cc}} = 0.95$ to the average of P_{cen} of 167 clusters sample we finally select. Second, we fit the distribution of the candidates of the central galaxy to obtain σ_{off} . There are five candidates of the central galaxy. We calculate the distribution of the projected distance between the most likely central galaxy and the 4 remaining central candidate galaxies, and fit this distribution with Equation (11). As shown in Figure 1, the red histogram shows the distribution of miscentering and the blue solid line represents the best fit curve. The best fit effective scale length is $\sigma_{\text{off}} = (0.095 \pm 0.002)\text{Mpc}$.

As a comparison, we also show the four free parameters model fitting results in APPENDIX A.

Substitute Equation (11) into following Equation (12), we can obtain the resulting mean surface mass profile for

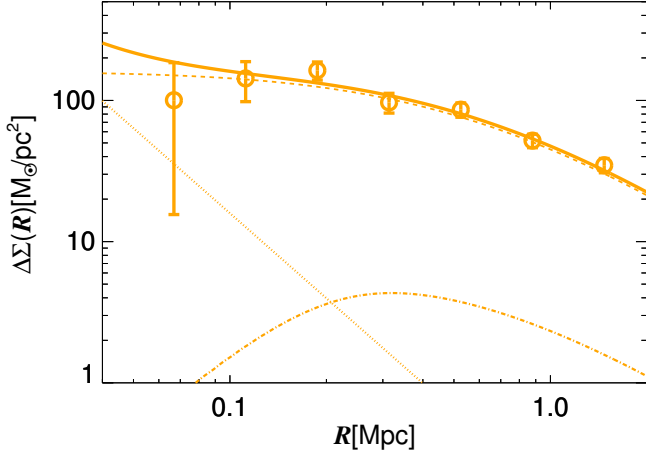


Figure 2. Best-fit model for weak lensing of 167 clusters. The orange circles represent the excess surface mass density $\Delta\Sigma(R)$ of cluster sample. Errors bars reflect the 68% confidence intervals obtained using bootstrapping. The solid line shows the best-fit model. The dashed line is the centered dark matter halo term. The dot-dashed line is the miscentering dark matter halo term and the dotted line corresponds to the stellar mass contribution from the central galaxy. The corresponding best-fit parameters are listed in Table 1.

the miscentered clusters.

$$\Sigma_{\text{NFW}}^{\text{off}}(R) = \int dR_{\text{mc}} P(R_{\text{mc}}) \Sigma_{\text{NFW}}(R|R_{\text{mc}}). \quad (12)$$

There are two free parameters M_{200} and C_{200} in our lensing fitting model.

3.2 Satellite number density

For each central galaxy, we count the number of galaxies in r -band magnitude range $17 < r_{\text{mag}} < 21$ and not brighter than the central galaxy in different projected radial bins. These galaxies contain satellites and galaxies in the background or foreground.

To compare directly with the weak lensing measurement, we calculate $\Delta\Sigma_g(R)$ instead of $\Sigma_g(R)$,

$$\Delta\Sigma_g(R) = \overline{\Sigma_g(< R)} - \overline{\Sigma_g(R)}, \quad (13)$$

where $\overline{\Sigma_g(< R)}$ represents galaxy surface number density within R , and $\overline{\Sigma_g(R)}$ is the average galaxy surface number density at the projected radius R and each of them contains the background galaxy density. So naturally the background is cancelled when we stack a lot of clusters. We calculate $\Delta\Sigma_g(R)$ for each individual cluster and average over the whole sample.

We assume the number density of galaxies also follow a NFW form as:

$$N(r) = \frac{N_0}{(r/r_{\text{s,gal}})(1+r/r_{\text{s,gal}})^2}. \quad (14)$$

The satellite galaxy surface number density fitting model includes the two components:

$$\Delta\Sigma_g(R) = P_{\text{cc}} \Delta\Sigma_g^{\text{cen}}(R) + (1 - P_{\text{cc}}) \Delta\Sigma_g^{\text{off}}(R). \quad (15)$$

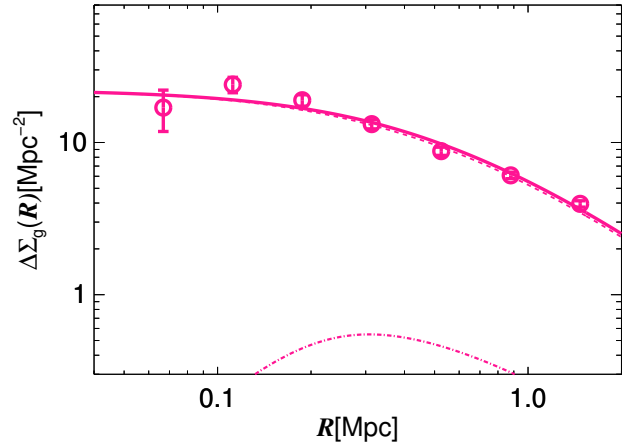


Figure 3. Best-fit model for galaxy number density of 167 clusters. The deep pink circles with errors bars represent the excess surface number density $\Delta\Sigma_g(R)$ of cluster sample. The solid line represents the best-fit model. The dashed line is the centered term and the dot-dashed line is the miscentering term. The corresponding best-fit parameters are listed in Table 2.

The two terms on the right side of the equation represent centered and miscentering NFW profile, respectively. N_0 , r_s are free parameters in our fitting. Owing to the same center we used both in weak lensing signal calculation and satellite galaxy count, the satellite number density profile shares the same σ_{off} and P_{cc} with density of mass. We fix $\sigma_{\text{off}} = 0.095 \text{Mpc}$, $P_{\text{cc}} = 0.95$.

4 RESULTS

With the Markov Chain Monte Carlo (MCMC) technique, we can fit the weak lensing signal and the satellite galaxy number density to get the posterior distribution of the free parameters.

In Figure 2, we show the stacked lensing signal of our cluster sample. The orange circles with errors bars represent weak lensing signal and errors bars reflect the 68% confidence intervals obtained by bootstrapping. The bold solid line shows the best-fit model, the dashed line is the centered dark matter halo term, the dot-dashed line is the miscentering dark matter halo term and the dotted line corresponds to the stellar mass contribution from central galaxy. The best fit parameters are listed in Table 1. We obtain a halo mass $M_{200} = 2.06^{+0.61}_{-0.41} \times 10^{14} M_{\odot}$ that is consistent with the halo mass fitting result in Miyatake et al. (2016), as well as the halo mass estimated by mass-richness relation in Melchior et al. (2017) and Shan et al. (2017) within 1σ error. The fitted scale radius is $r_s = 0.37^{+0.15}_{-0.10} \text{Mpc}$. The concentration parameter obtained here is $C_{200} = 2.80^{+0.81}_{-0.67}$. To compare our measurements with the three-dimensional (3D) N-body simulation results directly, we correct the C_{200} with the 3D correction in Giocoli et al. (2012):

$$C_{2\text{D}}(M) = C_{3\text{D}}(M) \times 1.630 M^{-0.018}, \quad (16)$$

and rescale the concentration parameter to $z = 0$ with the

Table 1. Best fit parameters of the mass profile from fitting the weak lensing data.

$M_{200}/10^{14}M_{\odot}$	C_{200}	$M_{\text{star}}/10^{11}M_{\odot}$	r_s/Mpc	χ^2/dof
$2.06^{+0.61}_{-0.41}$	$2.80^{+0.81}_{-0.67}$	4.99	$0.37^{+0.15}_{-0.10}$	4.15/5

Table 2. Best fit parameters of the galaxy density profile.

N_0/Mpc^{-3}	$r_{s,\text{gal}}/\text{Mpc}$	C_g	χ^2/dof
$68.17^{+13.60}_{-11.26}$	$0.34^{+0.04}_{-0.03}$	3.03 ± 0.30	12.27/5

redshift dependence in Klypin et al. (2016). We get the corrected concentration parameter $C_{200,3D} = 3.62^{+1.07}_{-0.88}$, which is consistent with the prediction from cosmological simulations provided by Klypin et al. (2016) within 1σ error.

In Figure 3, we show the excess surface number density of satellite galaxy of our cluster sample. The deep pink circles with errors bars are the satellite galaxy excess number surface density. The solid line represents the best-fit model. The dashed line is the centered term and the dot-dashed line is the miscentering term. Fitting results of excess surface number density are listed in Table 2.

We compare the satellite galaxy excess surface number density $\Delta\Sigma_g(R)$ with the mass excess surface density $\Delta\Sigma(R)$ directly in Figure 4. To compare their profiles intuitively, we divide 8.5 into $\Delta\Sigma(R)$ to obtain a similar amplitude with $\Delta\Sigma_g(R)$. As shown in Figure 4, they have similar distribution. We find that the fitted scale radius with satellite galaxy excess surface number density $r_{s,\text{gal}} = 0.34^{+0.04}_{-0.03}\text{Mpc}$ ($C_g = 3.03 \pm 0.30$) is consistent with the scale radius $r_s = 0.37^{+0.15}_{-0.10}\text{Mpc}$ ($C_{200} = 2.80^{+0.81}_{-0.67}$) fitted with weak lensing signal within 1σ error showing that the satellite galaxy number density profile traces mass distribution closely in the galaxy clusters.

In some previous studies, the generalized NFW or the Einasto parametric profile model is also used to fit the mass density or satellite galaxies number density profile (More et al. 2016; Lokas & Mamon 2003). In this paper, only the NFW profile model is adopted. Thus we also compare these two profiles in a non-parametric way without any model dependence. In Figure 5, we show the distribution of number-to-mass ratio with the projected radius R . Errors bars represent the 1σ uncertainties. The shaded region is standard errors of the number-to-mass ratio. The number-to-mass ratio is nearly a constant within 1σ error. Note that the number-to-mass ratio is still nearly a constant when projected distances are scaled by virial radii from the mass-richness scaling relation in Simet et al. (2017).

5 SUMMARY

In this short paper, we perform a comparison between the satellite number density profile and mass profile of redMaPPer clusters. For the mass profile, we select a sample of 167 redMaPPer clusters in the CS82 area with $20 < \lambda < 100$, $0.1 \leq z \leq 0.33$ and $P_{\text{cen}} > 0.7$ and calculate the stacked weak lensing signal around them to obtain the mass distribution from 0.03 Mpc to 1.5 Mpc. We extract the satellite galaxies in the same cluster sample using SDSS Stripe 82 photometric data in the r -band magnitude range $17 < r_{\text{mag}} < 21$. Comparing the excess surface mass density with the satellite galaxy number density, we find that they agree with each other well and can both be fitted with the NFW profile. The best-fit scale radius r_s and concentration parameter C of these two profiles are consistent with each other within 1σ error, thus we can conclude that the satellite galaxy number density is an unbiased tracers of mass distribution in galaxy clusters. Our conclusion is consistent with some similar studies using observational data based on dynamical methods (e.g. Carlberg et al. 1997; van der Marel et al. 2000; Biviano & Girardi 2003) or based on the other methods (e.g. Cirimele et al. 1997; Parker et al. 2005; Sereno et al. 2010).

ACKNOWLEDGEMENTS

We are indebted to the referee the thoughtful comments and insightful suggestions that improved this paper greatly. Based on observations obtained with MegaPrime/MegaCam, a joint project of CFHT and CEA/DAPNIA, at the CFHT, which is operated by the National Research Council (NRC) of Canada, the Institut National des Science de l'Univers of the Centre National de la Recherche Scientifique (CNRS) of France and the University of Hawaii. The Brazilian partnership on CFHT is managed by the Laboratrio Nacional de Astronomia (LNA). This work made use of the CHE cluster, managed and funded by ICRA/CBPF/MCTI, with financial support from FINEP and FAPERJ. We thank the support of the Laboratrio Interinstitucional de e-Astronomia (LIneA). We thank the CFHTLenS team for their pipeline development and verification upon which much of this surveys pipeline was built.

We acknowledge support from the National Key Program for Science and Technology Research and Development (2017YFB0203300). RL acknowledges NSFC grant (Nos. 11773032, 11333001), support from the Youth Innovation Promotion Association of CAS, Youth Science funding of NAOC and Nebula Talent Program of NAOC. LG acknowledges support from the NSFC grant (Nos. 11133003, 11425312), and a Newton Advanced Fellowship, as well as

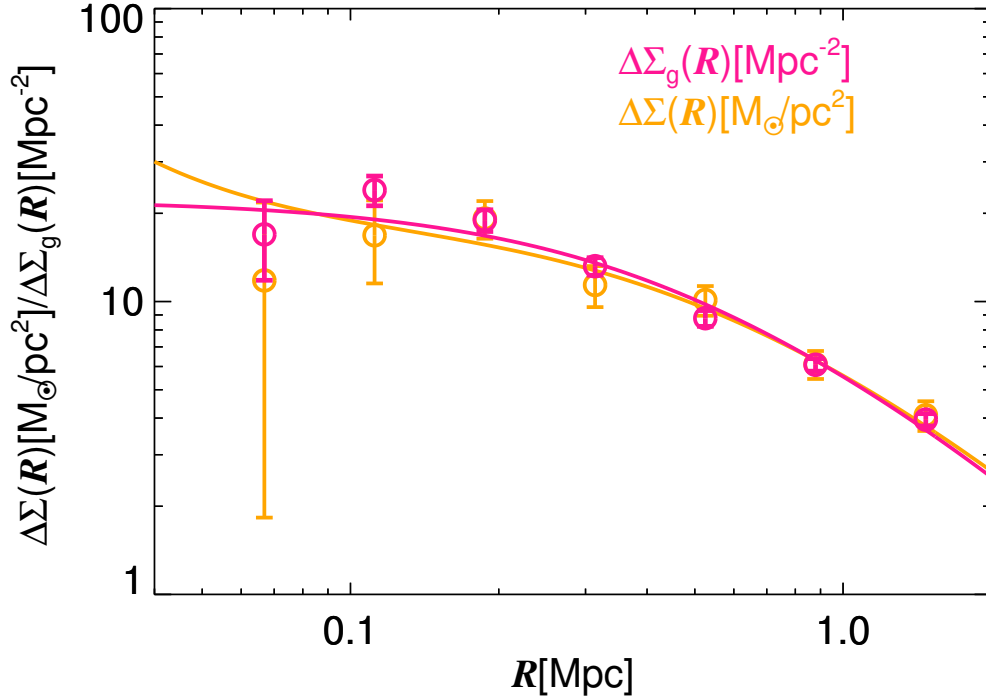


Figure 4. Comparison between mass distribution and galaxy number density profile. The deep pink circles with errors bars correspond to the satellite galaxy excess surface number density $\Delta\Sigma_g(R)$ and the deep pink solid line represents the best-fit model. Orange circles represent excess mass surface density $\Delta\Sigma(R)$ and the solid orange line represent the best-fit model. Errors bars reflect 1σ uncertainties. Here we divided 8.5 into $\Delta\Sigma(R)$ to get a similar amplitude with $\Delta\Sigma_g(R)$. Satellite galaxies are selected by $17 < r_{\text{mag}} < 21$.

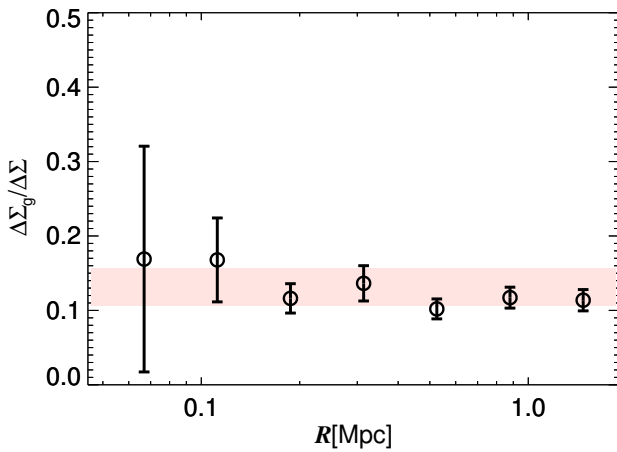


Figure 5. The distribution of number-to-mass ratio. Errors bars reflect the 1σ uncertainties. The shaded region is standard errors of the number-to-mass ratio.

the hospitality of the Institute for Computational Cosmology at Durham University. HYS and JPK acknowledge support from the ERC advanced grant LIDA. CXW and GC acknowledge NSFC grant No. 10903006, and support from the Middle-aged and Young Key Innovative Talents Program for Universities in Tianjin. M. Makler is partially supported by CNPq and FAPERJ. Fora Temer. T. Erben supported by the Deutsche Forschungsgemeinschaft in the framework of the TR33 ‘The Dark Universe’.

REFERENCES

- Abazajian K. N., et al., 2009, *ApJS*, 182, 543
Bahcall N. A., Kulier A., 2014, *MNRAS*, 439, 2505
Battaglia N., et al., 2016, *J. Cosmology Astropart. Phys.*, 8, 013
Benítez N., 2000, *ApJ*, 536, 571
Biviano A., Girardi M., 2003, *ApJ*, 585, 205
Budzynski J. M., Koposov S. E., McCarthy I. G., McGee S. L., Belokurov V., 2012, *MNRAS*, 423, 104
Bundy K., et al., 2015, *ApJS*, 221, 15
Carlberg R. G., Yee H. K. C., Ellingson E., 1997, *ApJ*, 478, 462
Carlberg R. G., Yee H. K. C., Morris S. L., Lin H., Hall P. B., Patton D. R., Sawicki M., Shepherd C. W., 2001, *ApJ*, 552, 427
Cirimele G., Nesci R., Trèvese D., 1997, *ApJ*, 475, 11
Coe D., Benítez N., Sánchez S. F., Jee M., Bouwens R., Ford H., 2006, *AJ*, 132, 926
Diemand J., Moore B., Stadel J., 2004, *MNRAS*, 352, 535
Erben T., et al., 2013, *MNRAS*, 433, 2545
Fischer P., Tyson J. A., 1997, *AJ*, 114, 14
Gao L., De Lucia G., White S. D. M., Jenkins A., 2004, *MNRAS*, 352, L1
Giocoli C., Meneghetti M., Ettori S., Moscardini L., 2012, *MNRAS*, 426, 1558
Hansen S. M., McKay T. A., Wechsler R. H., Annis J., Sheldon E. S., Kimball A., 2005, *ApJ*, 633, 122
Klypin A., Yepes G., Gottlöber S., Prada F., Heß S., 2016, *MNRAS*, 457, 4340
Kneib J.-P., et al., 2003, *ApJ*, 598, 804
Koranyi D. M., Geller M. J., Mohr J. J., Wegner G., 1998, *AJ*, 116, 2108
Leauthaud A., et al., 2012, *ApJ*, 744, 159
Li R., et al., 2014, *MNRAS*, 438, 2864
Li R., et al., 2016, *MNRAS*, 458, 2573

- Lin Y.-T., Mohr J. J., Stanford S. A., 2004, *ApJ*, 610, 745
 Lokas E. L., Mamon G. A., 2003, *MNRAS*, 343, 401
 Melchior P., et al., 2017, *MNRAS*, 469, 4899
 Miller L., Kitching T. D., Heymans C., Heavens A. F., van Waerbeke L., 2007, *MNRAS*, 382, 315
 Miller L., et al., 2013, *MNRAS*, 429, 2858
 Miyatake H., More S., Takada M., Spergel D. N., Mandelbaum R., Rykoff E. S., Rozo E., 2016, *Physical Review Letters*, 116, 041301
 More S., et al., 2016, *ApJ*, 825, 39
 Moustakas J., et al., 2013, *ApJ*, 767, 50
 Nagai D., Kravtsov A. V., 2005, *ApJ*, 618, 557
 Navarro J. F., Frenk C. S., White S. D. M., 1997, *ApJ*, 490, 493
 Parker L. C., Hudson M. J., Carlberg R. G., Hoekstra H., 2005, *ApJ*, 634, 806
 Popesso P., Biviano A., Böhringer H., Romaniello M., 2007, *A&A*, 464, 451
 Reis R. R. R., et al., 2012, *ApJ*, 747, 59
 Rines K., Geller M. J., Diaferio A., Mohr J. J., Wegner G. A., 2000, *AJ*, 120, 2338
 Rines K., Geller M. J., Kurtz M. J., Diaferio A., Jarrett T. H., Huchra J. P., 2001, *ApJ*, 561, L41
 Rozo E., Rykoff E. S., 2014, *ApJ*, 783, 80
 Rykoff E. S., et al., 2012, *ApJ*, 746, 178
 Rykoff E. S., et al., 2014, *The Astrophysical Journal*, 785, 104
 Sereno M., Lubini M., Jetzer P., 2010, *A&A*, 518, A55
 Shan H. Y., et al., 2014, *MNRAS*, 442, 2534
 Shan H., et al., 2017, *ApJ*, 840, 104
 Sheldon E. S., et al., 2009, *ApJ*, 703, 2232
 Simet M., McClintock T., Mandelbaum R., Rozo E., Rykoff E., Sheldon E., Wechsler R. H., 2017, *MNRAS*, 466, 3103
 Springel V., White S. D. M., Tormen G., Kauffmann G., 2001, *Monthly Notices of the Royal Astronomical Society*, 328, 726
 Squires G., Kaiser N., Fahlman G., Babul A., Woods D., 1996, *ApJ*, 469, 73
 Tustin A. W., Geller M. J., Kenyon S. J., Diaferio A., 2001, *AJ*, 122, 1289
 Tyson J. A., Fischer P., 1995, *ApJ*, 446, L55
 Velandar M., et al., 2014, *MNRAS*, 437, 2111
 Vogelsberger M., et al., 2014, *Nature*, 509, 177
 Wang W., Sales L. V., Henriques B. M. B., White S. D. M., 2014, *MNRAS*, 442, 1363
 Wojtak R., Lokas E. L., 2010, *MNRAS*, 408, 2442
 Yang X., Mo H. J., van den Bosch F. C., Weinmann S. M., Li C., Jing Y. P., 2005, *MNRAS*, 362, 711
 van der Marel R. P., Magorrian J., Carlberg R. G., Yee H. K. C., Ellingson E., 2000, *AJ*, 119, 2038

APPENDIX A: FOUR FREE PARAMETERS MODEL

In the lensing model, we can also treat σ_{off} and P_{cc} as free parameters. Thus, we have four free parameters in the fitting model, M_{200} , C_{200} , σ_{off} and P_{cc} . We show the 68 and 95 percent confidence intervals for the four free parameters in Figure A1. The last panel in each row shows the marginalized posterior distribution and the red solid lines represent the best fitting parameters. The red dashed lines are the 1σ error of σ_{off} and P_{cc} . The blue dashed lines represents the value of σ_{off} and P_{cc} in our two-parameters model.

For weak lensing data fitting, we obtain a halo mass $M_{200} = 2.15^{+0.38}_{-0.32} \times 10^{14} M_{\odot}$ and concentration parameter $C_{200} = 2.63^{+1.80}_{-0.61}$ which are consistent with our two-parameters model results in Section 3.1 within 1σ error. The best-fit results are listed in Table A1.

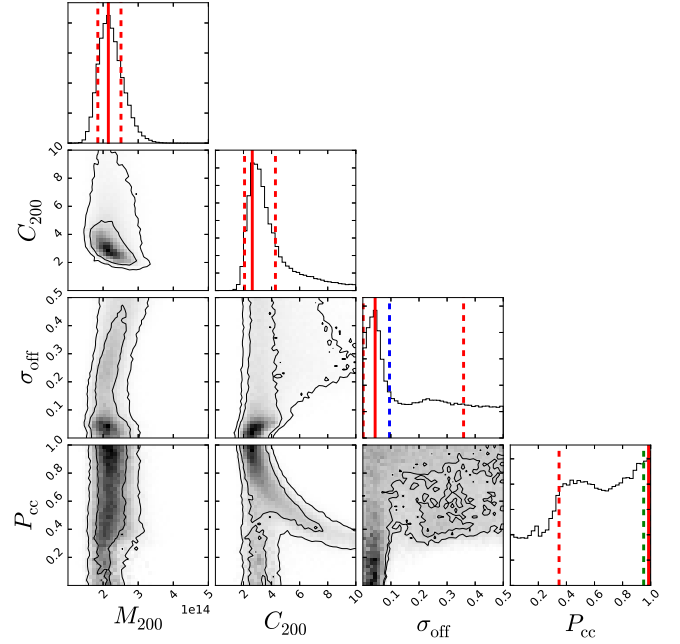


Figure A1. The 68 and 95 per cent confidence intervals for the four free parameters, M_{200} , C_{200} , σ_{off} and P_{cc} . M_{200} and σ_{off} are in units of M_{\odot} and Mpc, respectively. The last panel in each row shows the marginalized posterior distribution and the red solid lines represent the best fit parameters. The red dashed lines are the 1σ error of σ_{off} and P_{cc} . The blue dashed line is $\sigma_{\text{off}} = (0.095 \pm 0.002)\text{Mpc}$ and the green dashed line is $P_{\text{cc}} = 0.95$ which are the values we used in our two-parameter model.

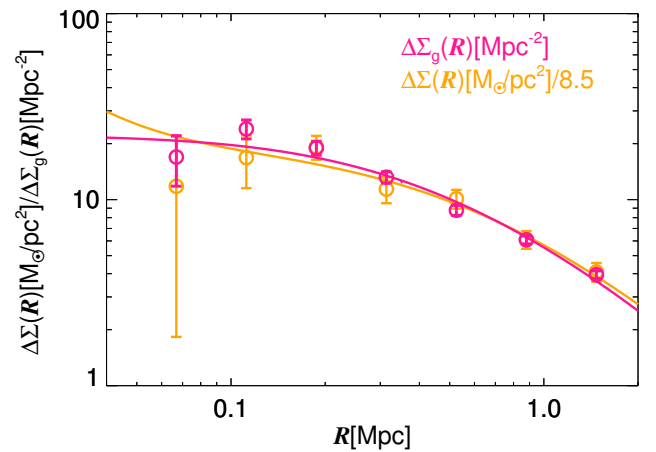


Figure A2. Similar figure to Figure 4, but with 4 free parameters.

As the satellite number density shares the same σ_{off} and P_{cc} with density of mass, we thus fix the two parameters to the best-fit value from weak lensing data for the satellite number density fitting. We show the best-fitting model of satellite number density in Table A2. Again, the best-fit scale radius from the galaxy density profile agrees with that from the lensing data (see Figure A2).

Table A1. Best fit parameters of the mass profile from fitting the weak lensing data

$M_{200}/10^{14}M_{\odot}$	C_{200}	$M_{\text{star}}/10^{11}M_{\odot}$	$\sigma_{\text{off}}/\text{Mpc}$	P_{cc}	r_s/Mpc	χ^2/dof
$2.15^{+0.38}_{-0.32}$	$2.63^{+1.80}_{-0.61}$	4.99	$0.04^{+0.32}_{-0.04}$	$0.99^{+0.01}_{-0.64}$	$0.32^{+0.10}_{-0.14}$	3.967/3

Table A2. Best fit parameters of the galaxy density profile.

N_0/Mpc^{-3}	$r_{\text{s,gal}}/\text{Mpc}$	C_g	χ^2/dof
$64.353^{+12.41}_{-10.47}$	$0.35^{+0.04}_{-0.03}$	2.98 ± 0.17	11.342/5

This paper has been typeset from a \LaTeX file prepared by the author.